ACS OMEGA

http://pubs.acs.org/journal/acsodf

Article

In Situ Growth of Metallic 1T-MoS_2 on TiO_2 Nanotubes with Improved Photocatalytic Performance

Miaogen Chen,* Tao Sun, Wan Zhao, Xiuru Yang, Wenya Chang, Xiaoxiao Qian, Qian Yang, and Zhi Chen*

Cite This: *ACS Omega* 2021, 6, 12787−12793

Read Online

ACCESS | Metrics & More | Article Recommendations | Supporting Information

ABSTRACT: 1T-MoS_2 is in situ grown on TiO_2 nanotubes (TNTs) using a hydrothermal method, forming a 1T-MoS_2@TNTs composite, which is confirmed by its physical characterization. The prepared composites show enhanced photocatalytic performance for the degradation of tetracycline hydrochloride under visible light, and the improved photocatalytic activity is closely related to the loaded amount of 1T-MoS_2. Therein, 0.5 wt % 1T-MoS_2@TNTs can degrade 57% in 1 h, which is the highest photocatalytic efficiency observed in experiments so far. It is speculated that the introduction of 1T-MoS_2 may optimize light absorption and charge separation/transport. The active species are identified and the reaction mechanism is proposed here.

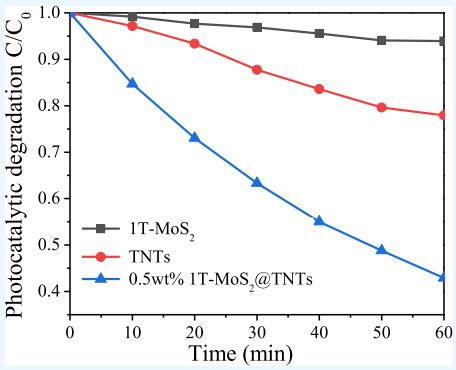

INTRODUCTION

Environmental pollution including water contamination is a serious problem threatening sustainable development. Antibiotic residue is one of the refractory pollutants in water, and diverse techniques have been evolved for efficient disposal.[1] Among these approaches, photocatalysis is one of the most attractive and booming methods because of its clean, nonpolluting, and efficient properties.[2] TiO_2 is one of the most investigated photocatalysts; however, it experiences the intrinsic limits of a wide band gap and fast recombination of photogenerated carriers. One of the widely used approaches is to construct a heterojunction for facing these obstacles.[2]

Recently, transition-metal sulfide MoS_2, a typical two-dimensional material with a graphene-like layered structure,[3] has attracted intense attention with wide applications.[4] Generally, MoS_2 has several polymorphs including metallic 1T and semiconducting 2H and 3R phases. Previous studies have mainly focused on 2H-MoS_2 due to its good stability, and the other two phases may convert into the 2H phase under specific conditions.[5] 2H-MoS_2 has been widely used as a high-performance photocatalyst, and intensive attempts have been made to improve its photocatalytic activity by modification or exfoliation.[6] Additionally, MoS_2 can work as an efficient cocatalyst by modifying other semiconductor photocatalysts such as TiO_2, which is one powerful strategy to realize highly efficient photocatalytic performances[7] by tuning the light absorption and the separation/transport of carrier.[8]

As is known, metallic 1T-MoS_2 has a single-layered S−Mo−S structure, in which each Mo atom is surrounded by six S atoms in an octahedral lattice.[9] Recently, 1T-MoS_2 has become a promising candidate for a wide range of applications due to its plentiful active sites and high electronic conductivity (6 orders of magnitude higher than that of 2H-MoS_2), exhibiting a better catalytic performance than the other semiconducting counterparts.[9] Lately, high-purity and stable 1T-MoS_2 nanosheets were synthesized using a hydrothermal method showing an excellent activity. 1T-MoS_2 may also work as a cocatalyst, which induces enhanced photocatalytic efficiency. Especially, its unique metallic feature may improve the separation/transport of carriers greatly,[10] which may lead to the potential replacement of Pt in practical applications.[11] However, the facile immobilization of 1T-MoS_2 on other semiconductor photocatalysts with improved performance is still a challenge.

To date, considerable efforts have been made to optimize the MoS_2 nanocomposites and expand their practical use.[12−14] For example, Zheng et al. applied a hierarchical MoS_2 nanosheet on a TiO_2 nanotube (TNT) array to enhance the photocatalytic and photocurrent performance.[12] Zhao et al. used the MoS_2 quantum dots@TNTs composites to improve the visible-light-driven high-efficiency photocatalysis.[13] In this work, 1T-MoS_2 is successfully grown on TNTs using an in situ hydrothermal method, which shows enhanced photocatalytic performance for the degradation of antibiotic residues in water.

Received: March 1, 2021
Accepted: April 21, 2021
Published: May 4, 2021

The prepared samples are characterized and the factors influencing the photocatalytic activity are discussed. The active species are studied and a reaction mechanism is suggested.

RESULTS AND DISCUSSION

Powder X-ray diffraction (XRD) patterns of the synthesized 1T-MoS_2, TNTs, and 1T-MoS_2@TNTs samples are shown in Figure 1a. It is noticed that metallic 1T-MoS_2 has two obvious

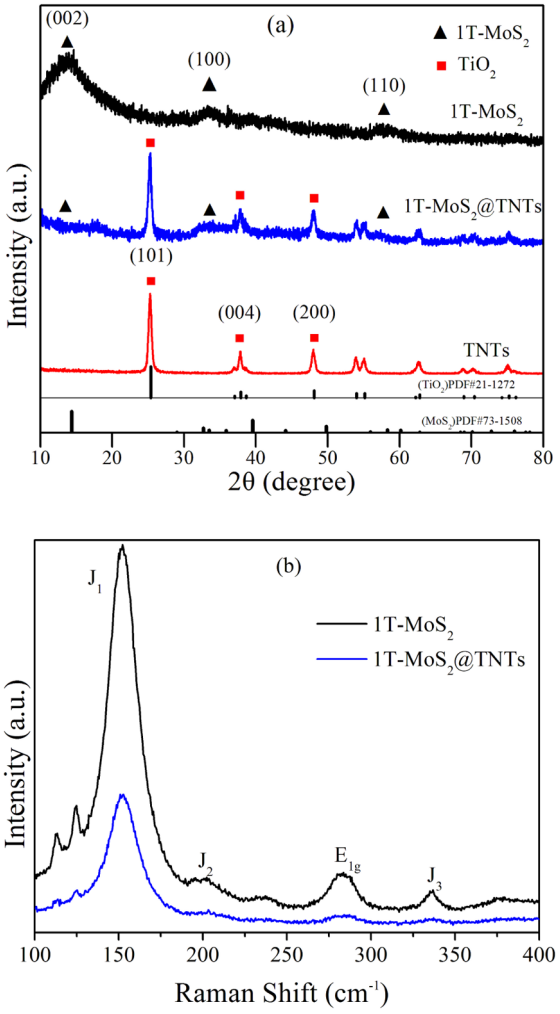

Figure 1. (a) XRD patterns of prepared 1T-MoS_2, TNTs, and 1T-MoS_2@TNTs; (b) Raman spectra of 1T-MoS_2 and 1T-MoS_2@TNTs.

characteristic peaks located at 13.9 and 33.2°, which could be assigned to its (002) and (100) facets.[9] The peak of the (002) facet is much greater than that of the (100) facet, indicating that the prepared 1T-MoS_2 sample has a well-crystallized (002) facet.[15] As shown, the characteristic peaks of TNTs are completely consistent with that of anatase TiO_2,[16] which illustrates that the obtained TNTs are anatase with good crystallinity.[17] As for 1T-MoS_2@TNTs, the characteristic diffraction peaks of TNTs are all present without an obvious decrease of the relative peak intensity, which indicates that the growth of 1T-MoS_2 does not destroy the crystal structure of TiO_2. Additionally, quite weak diffraction peaks are also observed, which may come from the immobilized 1T-MoS_2.

Raman spectra are obtained to further identify the existence and the phase characteristics of the prepared 1T-MoS_2 and 1T-MoS_2@TNTs. As shown in Figure 1b, the characteristic peaks at 151, 201, 283, and 337 cm^{-1} are observed, which could be attributed to the J_1, J_2, E_{1g}, and J_3 of 1T-MoS_2, respectively. Moreover, no obvious E_{2g} peak of 2H-MoS_2 is observed at 380 cm^{-1}.[11] These results indicate that 1T-MoS_2 is obtained and successfully grown and immobilized on TNTs.

Furthermore, X-ray photoelectron spectroscopy (XPS) is employed to analyze the prepared samples, as shown in Figures 2 and S1. As shown in Figure S1a, all the elements of Mo, S, Ti, and O are present, suggesting the successful immobilization of 1T-MoS_2 on TNTs. As shown in Figure 2a, two main deconvoluted peaks are observed at 227.4 and 230.6 eV on the Mo 3d spectra, which correspond to $3d_{3/2}$ and $3d_{5/2}$ of Mo^{4+} species.[17] The other two peaks at the binding energies of 231.8 and 234.7 eV belong to Mo^{6+}, which may come from the unreacted MoO_3 or the oxidized MoS_2 in air.[15] Additionally, two weak peaks at 225.3 and 228.2 eV may belong to Mo^{3+}, which should be derived from the S vacancy in MoS_2 and/or the formed crystal defects.[16] As shown in Figure 2b, the peaks at 161.8 and 160.5 eV could be assigned to $2p_{3/2}$ and $2p_{1/2}$ of S^{2-} from MoS_2.[9] The other peaks at 168.7 and 167.6 eV can be assigned to $2p_{1/2}$ and $2p_{3/2}$ of S^{4+} in sulfate groups (SO_3^{2-}).[18] Figure 2c shows two peaks at 463.6 and 457.8 eV, which could be attributed to Ti 2p of 1T-MoS_2@TNTs. As shown in Figure 2d, two O 1s peaks at 530.5 and 529.1 eV are present. The first peak corresponds to the O atom bonded to Ti, and the latter one is ascribed to the surface hydroxyl species.[19] Compared with the curves in Figure S1b,c, it could be seen that both binding energies of Ti 2p and O 1s 1T-MoS_2@TNTs are slightly shifted, which indicates the existence of electron interaction between 1T-MoS_2 and TNTs.

Scanning electron microscopy (SEM) images and energy-dispersive spectrometry (EDS) mapping images are used to investigate the surface morphology and elemental distribution of 1T-MoS_2@TNTs, as shown in Figure 3. As shown in Figure 3a, TiO_2 has an obvious one-dimensional morphology with diameters of about 10 nm. The existence of MoS_2 is identified by the EDS mapping from an arbitrarily selected area, shown in Figure 3b−g. As shown, all the elements including Mo and S are evenly distributed in the 1T-MoS_2@TNTs composites. In addition, no aggregated particles are observed on the surface of TNTs. It indicates that 1T-MoS_2 has been successfully grown on the TiO_2 surface with good dispersion.

Transmission electron microscopy (TEM) and high-resolution TEM (HRTEM) are applied to investigate the microstructure of the stable 1T-MoS_2@TNTs composites, as shown in Figure 4. Figure 4a shows that 1T-MoS_2@TNTs are completely composed of nanotubes with a diameter of about 7.5 nm. HRTEM images are shown in Figure 4b−d, and a more obvious tubular structure is observed in Figure 4b. The different contrast at the tube wall is also present, which might be derived from the loaded 1T-MoS_2. For further understanding, high-resolution pictures of the circled parts in Figure 4b are given in Figure 4c,d. The lattice of the light part is 0.35 nm, which could be assigned to the (101) facet of TiO_2. The tube wall is composed of several-layered TiO_2, and the thickness of each layer is about 0.72 nm. As for Figure 4d, lattice fringes with a width of 0.26 nm can be attributed to the (100) facet of MoS_2, which is at an angle of 120° from the TiO_2 (101) facet.[20] To get further information about 1T-MoS_2 in 1T-MoS_2@TNTs, the selected zone in Figure S2a was filtered by fast Fourier transform filtration to remove the irrelevant noise based on the previous image-processing procedure.[21] The obtained atomic arrangement diagram and

https://doi.org/10.1021/acsomega.1c01068
ACS Omega 2021, 6, 12787−12793

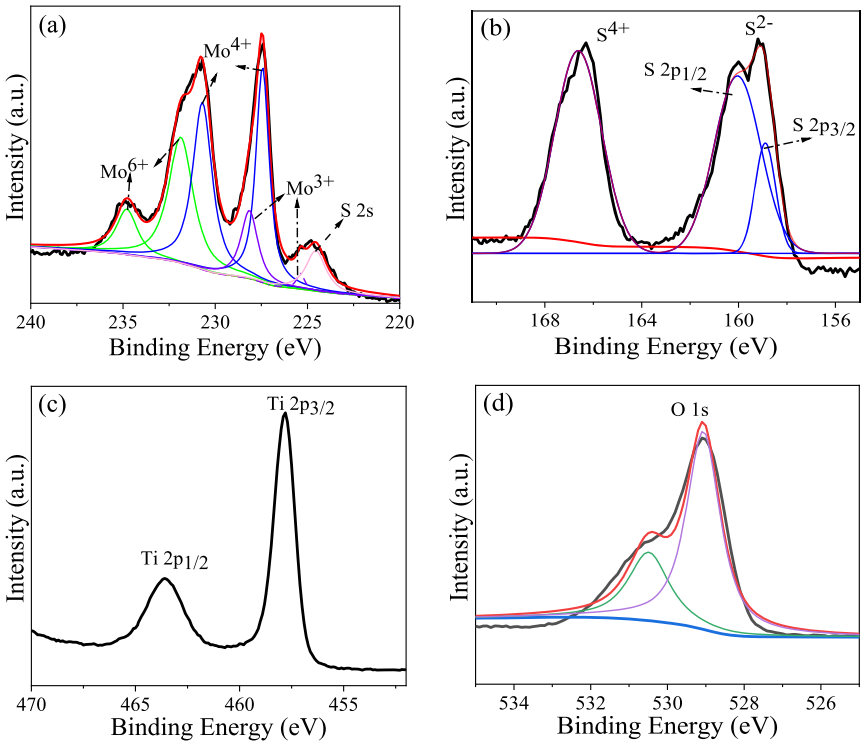

Figure 2. XPS spectra of (a) Mo 3d, (b) S 2p, (c) Ti 2p, and (d) O 1s on 1T-MoS_2@TNTs.

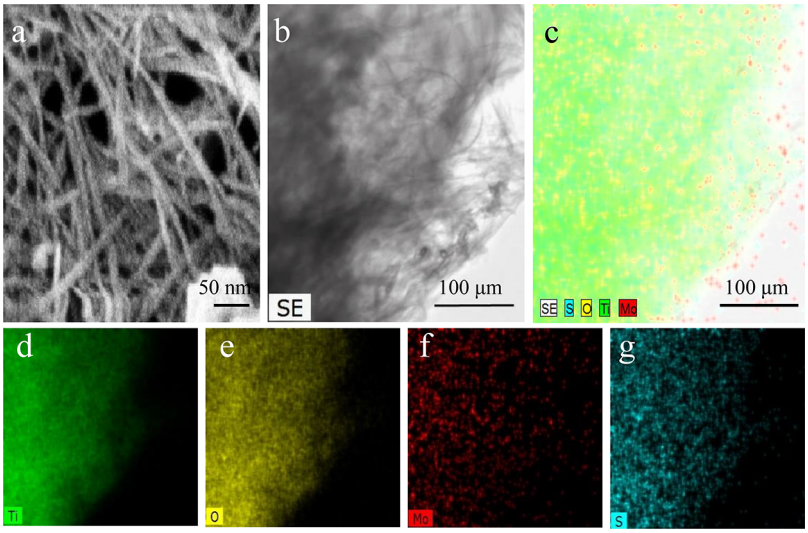

Figure 3. (a) SEM image of 1T-MoS_2@TNTs and (b) SEM images with the corresponding elemental mapping images of (c) all elements, (d) Ti, (e) O, (f) Mo, and (g) S.

lattice dislocation are shown in Figure S2b,c, respectively. The characteristic trigonal lattice is evidently seen in Figure S2a and the hexagonal atomic arrangement of Mo of MoS_2 is seen in Figure S2b, which confirms that the obtained MoS_2 has the 1T phase.[21] Figure S2c shows the lattice fringes in the same direction with obvious dislocations indicating the presence of defects in 1T-MoS_2, which is in correspondence with the above XPS results. Additionally, the *a* and *b* vectors give a length of 3.15 Å, which indicates that one Mo atom may be surrounded by six S atoms, as shown in Figure S2d.

The light response of the obtained samples is analyzed by UV−vis diffuse reflectance spectroscopy, as shown in Figure 5a. Compared to TNTs, 1T-MoS_2@TNTs has stronger absorption in the visible region. At the same time, slight red shifts of the spectrum could be observed for 1T-MoS_2@TNTs as shown in Figure S3a, which indicates that the interaction between 1T-MoS_2 and TNTs may influence the band energy.[20] The band gaps of prepared photocatalysts are calculated by using the Tauc equation,[9] shown in Figures 5b and S3b. The band gap of TNTs is 3.17 eV. However, the band gap of 1T-MoS_2@TNTs is decreased to 3.09 eV. More decreases are observed by further increasing the contents of 1T-MoS_2 and the values are 3.05, 3.03, and 2.84 eV for 1.0 wt % 1T-MoS_2@TNTs, 1.5 wt % 1T-MoS_2@TNTs, and 2.0 wt % 1T-MoS_2@TNTs (see Figure S3b), respectively. It is speculated that the

https://doi.org/10.1021/acsomega.1c01068
ACS Omega 2021, 6, 12787−12793

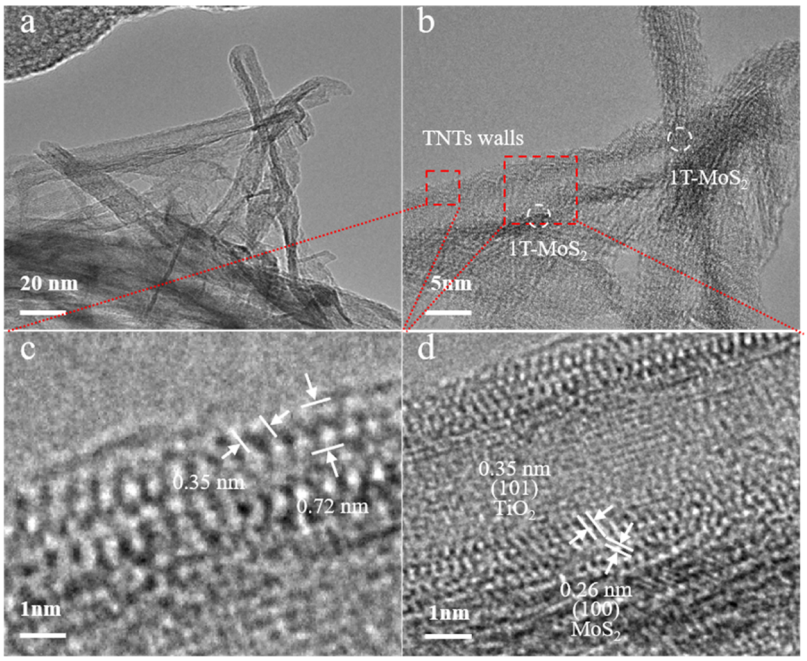

Figure 4. (a,b) HRTEM images of the 1T-MoS_2@TNTs composite; (c,d) enlarged images of the selected zone.

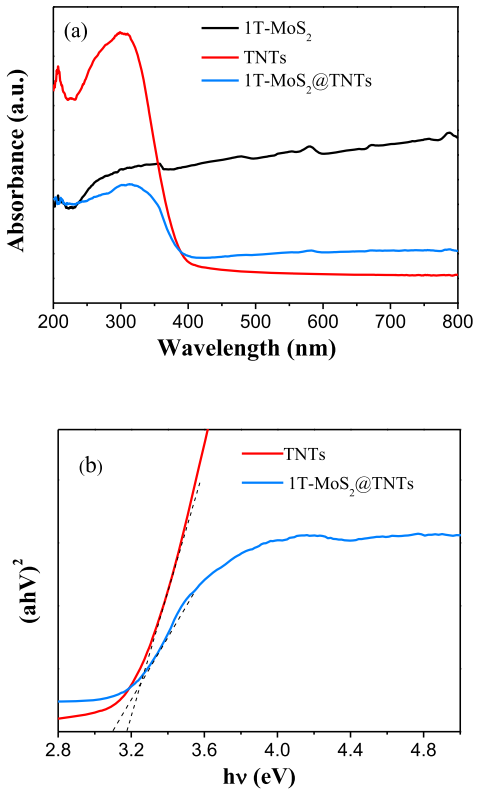

Figure 5. (a) UV−vis diffuse reflectance spectra and (b) band gap of TNTs and 1T-MoS_2@TNTs.

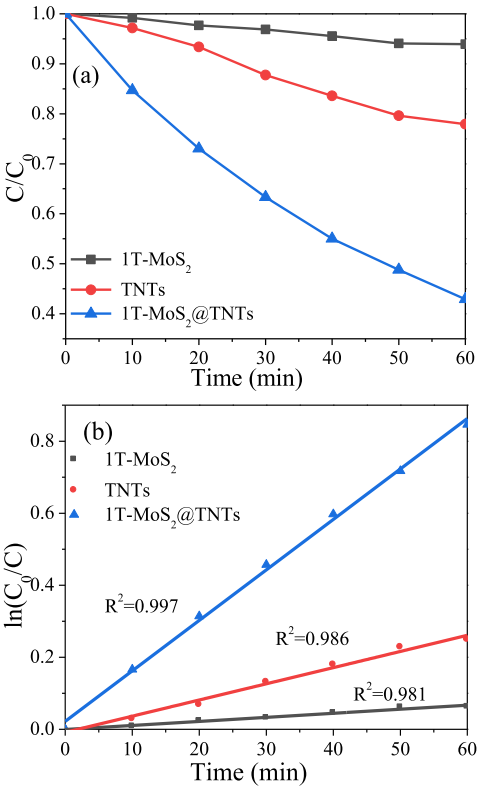

Figure 6. (a) Photocatalytic degradation of TC-HCl by 1T-MoS_2, TNTs, and 1T-MoS_2@TNTs and (b) pseudo-first-order kinetics fitting of the photodegradation.

narrower band gap may improve the light harvesting, which facilitates enhanced photocatalytic activity.

The degradation of tetracycline hydrochloride (TC-HCl) under visible light is carried out to investigate the photocatalytic performance of the obtained samples, as shown in Figure 6a. Pristine 1T-MoS_2 and TNTs can only degrade about 10 and 23% TC-HCl in 1 h, respectively. In contrast, 1T-MoS_2@TNTs (0.5 wt %) can degrade 57% TC-HCl under the same conditions, which is higher than previously reported efficiencies of 15 and 25%.[9,14] In addition, Figure S4 shows the degradation curves of 1T-MoS_2@TNTs with different loaded amounts of 1T-MoS_2, where it is observed that the prepared 0.5 wt % 1T-MoS_2@TNTs exhibits the highest catalytic activity. The pseudo-first-order kinetics fitting of the photo-

https://doi.org/10.1021/acsomega.1c01068
ACS Omega 2021, 6, 12787−12793

degradation is given in Figure 6b. The reaction rate constants k of TC-HCl decomposition are 1.1×10^{-3} and 4.4×10^{-3} min^{-1} for 1T-MoS_2 and TNTs, respectively. Enhanced reaction rates are observed for 1T-MoS_2-loaded photocatalysts, and a maximum of 140 min^{-1} is achieved for 1T-MoS_2@TNTs (0.5 wt %), which is 12.7 and 3.2 times more than those of 1T-MoS_2 and TNTs. The full-wavelength absorption spectra of TC-HCl during degradation on 1T-MoS_2@TNTs are shown in Figure S5. The absorption from TC-HCl is clearly observed and the absorption intensity decreases along with the reaction, indicating that no other intermediates are formed. Cyclic experiments for TC-HCl photodegradation have been conducted and the degradation rate is found to be reduced from 56.2 to 36.8% after four cycles, as shown in Figure S6.

Trapping experiments are performed to figure out the active ingredients in the photocatalytic process by using 1T-MoS_2@TNTs as the photocatalyst, as shown in Figure 7. Ethyl-

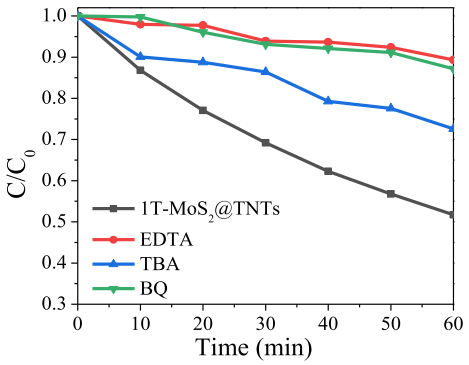

Figure 7. Photocatalytic degradation of TC-HCl over 1T-MoS_2@TNTs without and with addition of EDTA, TBA, and BQ.

enediaminetetraacetic acid (EDTA), benzoquinone (BQ), and *tert*-butyl alcohol (TBA) are used to scavenge the holes (h^+), superoxide ($^\bullet O_2^-$) radicals, and hydroxyl ($^\bullet OH$) radicals, respectively. 10.0 mg of the photocatalyst is used and the operation is similar to the above photodegradation processes. After the addition of EDTA, BQ, and TBA, the degradation efficiency is obviously reduced, which indicates that h^+, $^\bullet O_2^-$, and $^\bullet OH$ may be the active species and responsible for the catalytic reaction.

Photocurrent response and electrochemical impedance spectroscopy (EIS) are employed to analyze the charge transfer in the photocatalytic process. As shown in Figure 8a, the 1T-MoS_2@TNTs composite has a much stronger photocurrent than the pristine 1T-MoS_2 and TNTs. This indicates that 1T-MoS_2@TNTs photocatalyst has better charge separation efficiency, which accounts for its higher activity. EIS is used to further clarify the charge transport on the prepared samples, as shown in Figure 8b. 1T-MoS_2@TNTs displays a much smaller EIS arc radius than TNTs, which indicates that the addition of metallic 1T-MoS_2 to TNTs can reduce the resistance of TNTs.[20]

The band structures of TNTs and 1T-MoS_2 are obtained from the Mott−Schottky results in Figure S7, which indicate that they are all n-type semiconductors.[16] Together with the above discussions, a mechanism is proposed for the photodegradation of TC-HCl on 1T-MoS_2@TNTs, as shown in Figure 9. The potentials of CB and VB of 1T-MoS_2 are 0.18 and 1.98 eV, and those of TNTs are −0.4 and 2.8 eV, respectively. The electrons are excited to the CB of TiO_2 under

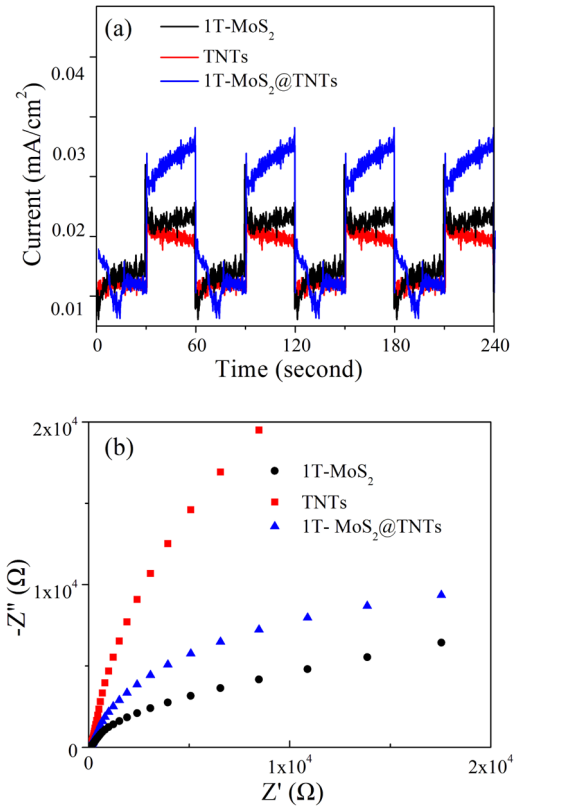

Figure 8. (a) Typical photocurrent response and (b) EIS spectra of samples 1T-MoS_2, TNTs, and 1T-MoS_2@TNTs.

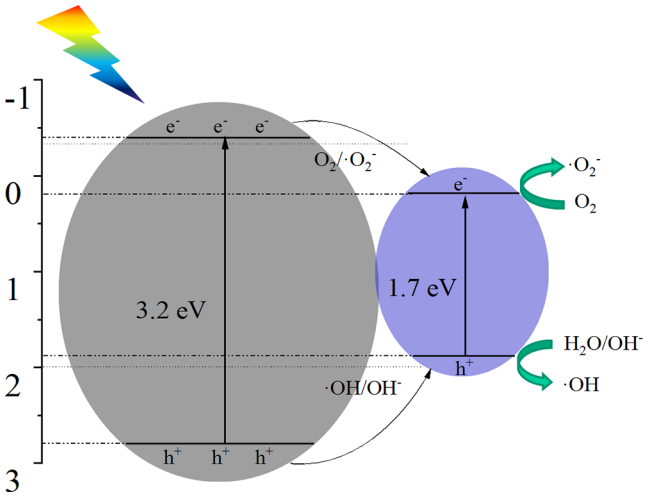

Figure 9. Schematic illustrations for the photogenerated charge carrier transfer on 1T-MoS_2@TNTs.

visible-light irradiation and migrated to the CB of 1T-MoS_2 through the formed interface. Meanwhile, the holes in the VB of TiO_2 may transfer to the VB of 1T-MoS_2. Consequently, a type I heterojunction may be formed in the 1T-MoS_2@TNTs composite, which optimizes the photocatalytic activity by improving the charge separation.[22]

CONCLUSIONS

In summary, 1T-MoS_2@TNTs composites have been successfully constructed by the in situ growth of 1T-MoS_2 on the TNTs using a hydrothermal process, which show enhanced

https://doi.org/10.1021/acsomega.1c01068
ACS Omega 2021, 6, 12787−12793

photocatalytic performance for the degradation of TC-HCl under visible light. The improved photocatalytic activity is closely related to the loaded amount of 1T-MoS_2, and the highest photocatalytic efficiency is observed on 0.5 wt % 1T-MoS_2@TNTs. The introduction of 1T-MoS_2 may optimize light absorption and charge separation/transport. The active species are identified and a reaction mechanism is proposed. This work may provide an alternative for the construction of a new photocatalyst and also a new direction for application of 1T-MoS_2 in the energy and environmental fields.

MATERIALS AND METHODS

Synthesis of 1T-MoS_2. The preparation of 1T-MoS_2 was conducted according to the modified method from ref 8. Typically, 1.96 mg MoO_3, 0.10 g thioacetic acid (TAA), and 0.96 g urea were dissolved in 80.0 mL of deionized water and stirred magnetically (with a cylindrical stirring bar, 8 × 35 mm) for 2 h at a speed of 400 rpm. Then, the solution was sealed in an autoclave and heated at 200 °C for 12 h. After that, the solution was cooled down to room temperature, and the solid product was collected and washed with deionized water several times. The prepared 1T-MoS_2 was dispersed in deionized water before further use.

Synthesis of TNTs. TNTs were prepared using a hydrothermal method.[23] Typically, 0.96 g of urea and 1.92 g of titanium sulfate were dissolved in 80.0 mL of deionized water and stirred for 2 h. Then, the solution was transferred into a reaction vessel and reacted at 220 °C for 12 h to obtain TiO_2 powder. The obtained TiO_2 powder was added to 100.0 mL of 10.0 mol/L NaOH solution and stirred for 4 h. Then, the solution was transferred into a Teflon container and heated at 150 °C for 12 h. After washing with a 0.1 mol/L HNO_3 aqueous solution and deionized water, white products were obtained and ground into powder for further use.

Synthesis of 1T-MoS_2@TiO_2. 400 mg TiO_2 powder was added into the mixed solution containing 2.1 mg TAA, 18 mg urea, and 1.8 mg MoO_3 and stirred for 2 h. Then, the solution was sealed in an autoclave and heated at 200 °C for 12 h. After that, the solution was cooled down to room temperature, and the solid product was collected and washed with deionized water several times. The obtained samples were named as 1T-MoS_2@TNTs (the content of 1T-MoS_2 is 0.5 wt %). Other samples with different MoS_2 contents were similarly synthesized by changing the concentrations of MoO_3 precursors (Supporting Information).

Characterization. XRD was conducted at a scan rate of 10°/min on a Bruker D2 PHASER with Cu Kα-radiation. XPS was obtained on the Axis Supra XPS instrument using Al Kα as the source. SEM was conducted on a FE-SEM S-4800 (Hitachi). TEM was carried out on the FEI F200S equipment at an accelerating voltage of 200 kV.

Photoelectrochemical Measurements. Electrochemical testing was carried out on the CHI 660E electrochemical workstation. 15.0 mg prepared MoS_2, TNTs, and 1T-MoS_2@TNTs were separately dissolved in 3 mL of polyvinylidene fluoride solution and coated on the fluorine-doped tin oxide conducting glass by spin coating to form an electrode, respectively. A 300 W xenon lamp was used as the light source for photocurrent testing.

Photocatalytic Performance. The photocatalytic performance was studied by degrading the TC-HCl solution under visible light as the model reaction. A 300 W xenon lamp worked as the light source in the wavelength range of 420−780 nm, and the distance between the lamp and liquid level was set as 15 cm. 1.0 mg of the photocatalyst was dispersed in 100.0 mL of 20.0 mg/L TC-HCl solution. The reaction solution was stirred magnetically at a speed of 200 rpm in the dark for 1 h to achieve adsorption−desorption equilibrium. The concentration of TC-HCl was investigated at its maximum adsorption of 356 nm on the UV 2600 spectrophotometer. The pH values of the solution before and after the reaction are 4.23 and 4.28, respectively, and not much difference is observed.

ASSOCIATED CONTENT

Supporting Information

The Supporting Information is available free of charge at https://pubs.acs.org/doi/10.1021/acsomega.1c01068.

XPS and HRTEM spectra of 1T-MoS_2@TNTs; UV−vis diffuse reflectance spectra, band gaps, and Mott−Schottky curves of TNTs and 1T-MoS_2; and photocatalytic degradation of TC-HCl of TNTs and 1T-MoS_2@TNTs composites with different loaded amounts of 1T-MoS_2 (PDF)

AUTHOR INFORMATION

Corresponding Authors

Miaogen Chen − *Key Laboratory of Intelligent Manufacturing Quality Big Data Tracing and Analysis of Zhejiang Province, Department of Physics, China Jiliang University, Hangzhou 310018, China*; orcid.org/0000-0003-1930-8331; Email: phycmg@cjlu.edu.cn

Zhi Chen − *College of Materials and Chemistry, China Jiliang University, Hangzhou 310018, China*; Email: zchen@cjlu.edu.cn

Authors

Tao Sun − *Key Laboratory of Intelligent Manufacturing Quality Big Data Tracing and Analysis of Zhejiang Province, Department of Physics, China Jiliang University, Hangzhou 310018, China*

Wan Zhao − *College of Materials and Chemistry, China Jiliang University, Hangzhou 310018, China*

Xiuru Yang − *College of Materials and Chemistry, China Jiliang University, Hangzhou 310018, China*

Wenya Chang − *Key Laboratory of Intelligent Manufacturing Quality Big Data Tracing and Analysis of Zhejiang Province, Department of Physics, China Jiliang University, Hangzhou 310018, China*

Xiaoxiao Qian − *College of Materials and Chemistry, China Jiliang University, Hangzhou 310018, China*

Qian Yang − *College of Materials and Chemistry, China Jiliang University, Hangzhou 310018, China*

Complete contact information is available at: https://pubs.acs.org/10.1021/acsomega.1c01068

Notes

The authors declare no competing financial interest.

ACKNOWLEDGMENTS

This research was supported by the National Key R&D Program of China (grant no. 2019YFE0112000), Zhejiang Natural Science Foundation of China (grant no. LY17E020008), Fundamental Research Funds for the Provincial Universities of Zhejiang (grant no. 2020YW53), Department of Education of Zhejiang Province (grant no.

Y202045252), and Opening Project of State Key Laboratory of High-Performance Ceramics and Superfine Microstructure (grant no. SKL201803SIC).

REFERENCES

(1) Palominos, R. A.; Mondaca, M. A.; Giraldo, A.; Peñuela, G.; Pérez-Moya, M.; Mansilla, H. D. Photocatalytic oxidation of the antibiotic tetracycline on TiO_2 and ZnO suspensions. *Catal. Today* **2009**, *144*, 100−105.

(2) Zhou, D.; Chen, Z.; Yang, Q.; Dong, X.; Zhang, J.; Qin, L. In-situ construction of all-solid-state Z-scheme g-C_3N_4/TiO_2 nanotube arrays photocatalyst with enhanced visible-light-induced properties. *Sol. Energy Mater. Sol. Cells* **2016**, *157*, 399−405.

(3) Quinn, M. D. J.; Ho, N. H.; Notley, S. M. Aqueous dispersions of exfoliated molybdenum disulfide for use in visible-light photocatalysis. *ACS Appl. Mater. Interfaces* **2013**, *5*, 12751−12756.

(4) Hu, C.; Zheng, S.; Lian, C.; Chen, F.; Lu, T.; Hu, Q.; Duo, S.; Zhang, R.; Guan, C. α-S nanoparticles grown on MoS_2 nanosheets: A novel sulfur-based photocatalyst with enhanced photocatalytic performance. *J. Mol. Catal. A: Chem.* **2015**, *396*, 128−135.

(5) Lukowski, M. A.; Daniel, A. S.; Meng, F.; Forticaux, A.; Li, L.; Jin, S. Enhanced hydrogen evolution catalysis from chemically exfoliated metallic MoS_2 nanosheets. *J. Am. Chem. Soc.* **2013**, *135*, 10274−10277.

(6) Xu, H.; Han, D.; Bao, Y.; Cheng, F.; Ding, Z.; Tan, S. J. R.; Loh, K. P. Observation of Gap Opening in 1T′ Phase MoS_2 Nanocrystals. *Nano Lett.* **2018**, *18*, 5085−5090.

(7) Adams, L. K.; Lyon, D. Y.; Alvarez, P. J. J. Comparative eco-toxicity of nanoscale TiO_2, SiO_2, and ZnO water suspensions. *Water Res.* **2006**, *40*, 3527−3532.

(8) Zhou, D.; Chen, Z.; Yang, Q.; Shen, C.; Tang, G.; Zhao, S.; Zhang, J.; Chen, D.; Wei, Q.; Dong, X. Facile Construction of g-C_3N_4 Nanosheets/TiO_2 Nanotube Arrays as Z-Scheme Photocatalyst with Enhanced Visible-Light Performance. *ChemCatChem* **2016**, *8*, 3064−3073.

(9) Yang, X.; Chen, Z.; Fang, J.; Yang, Q.; Zhao, W.; Qian, X.; Liu, C.; Zhou, D.; Tao, S.; Liu, X. Efficient exfoliation to MoS_2 nanosheets by salt-assisted refluxing and ultrasonication with photocatalytic application. *Mater. Lett.* **2019**, *255*, 126596.

(10) Guayaquil-Sosa, J. F.; Serrano-Rosales, B.; Valadés-Pelayo, P. J.; de Lasa, H. Photocatalytic hydrogen production using mesoporous TiO_2 doped with Pt. *Appl. Catal., B* **2017**, *211*, 337−348.

(11) Geng, X.; Sun, W.; Wu, W.; Chen, B.; Al-Hilo, A.; Benamara, M.; Zhu, H.; Watanabe, F.; Cui, J.; Chen, T.-p. Pure and stable metallic phase molybdenum disulfide nanosheets for hydrogen evolution reaction. *Nat. Commun.* **2016**, *7*, 10672.

(12) Zheng, L.; Han, S.; Liu, H.; Yu, P.; Fang, X. Hierarchical MoS_2 nanosheet@TiO_2 nanotube array composites with enhanced photocatalytic and photocurrent performances. *Small* **2016**, *12*, 1527−1536.

(13) Zhao, F.; Rong, Y.; Wan, J.; Hu, Z.; Peng, Z.; Wang, B. MoS_2 quantum dots@TiO_2 nanotube composites with enhanced photo-excited charge separation and high-efficiency visible-light driven photocatalysis. *Nanotechnology* **2018**, *29*, 105403.

(14) Zhao, W.; Liu, X.; Yang, X.; Liu, C.; Qian, X.; Sun, T.; Chang, W.; Zhang, J.; Chen, Z. Synthesis of novel 1T/2H-MoS_2 from MoO_3 nanowires with enhanced photocatalytic performance. *Nanomaterials* **2020**, *10*, 1124.

(15) Sheng, B.; Liu, J.; Li, Z.; Wang, M.; Zhu, K.; Qiu, J.; Wang, J. Effects of excess sulfur source on the formation and photocatalytic properties of flower-like MoS_2 spheres by hydrothermal synthesis. *Mater. Lett.* **2015**, *144*, 153−156.

(16) Guo, L.; Yang, Z.; Marcus, K.; Li, Z.; Luo, B.; Zhou, L.; Wang, X.; Du, Y.; Yang, Y. MoS_2/TiO_2 heterostructures as nonmetal plasmonic photocatalysts for highly efficient hydrogen evolution. *Energy Environ. Sci.* **2018**, *11*, 106−114.

(17) Sakashita, Y.; Yoneda, T. Orientation of MoS_2 Clusters Supported on Two Kinds of γ-Al_2O_3 Single Crystal Surfaces with Different Indices. *J. Catal.* **1999**, *185*, 487−495.

(18) Hu, W.-H.; Shang, X.; Xue, J.; Dong, B.; Chi, J.-Q.; Han, G.-Q.; Liu, Y.-R.; Li, X.; Yan, K.-L.; Chai, Y.-M.; Liu, C.-G. Activating MoS_2/CNs by tuning (001) plane as efficient electrocatalysts for hydrogen evolution reaction. *Int. J. Hydrogen Energy* **2017**, *42*, 2088−2095.

(19) Zhou, J.; Yin, L.; Li, H.; Liu, Z.; Wang, J.; Duan, K.; Qu, S.; Weng, J.; Feng, B. Heterojunction of $SrTiO_3$/TiO_2 nanotubes with dominant (001) facets: Synthesis, formation mechanism and photoelectrochemical properties. *Mater. Sci. Semicond. Process.* **2015**, *40*, 107−116.

(20) Zhang, J.; Huang, L.; Lu, Z.; Jin, Z.; Wang, X.; Xu, G.; Zhang, E.; Wang, H.; Kong, Z.; Xi, J.; Ji, Z. Crystal face regulating MoS_2/TiO_2(001) heterostructure for high photocatalytic activity. *J. Alloys Compd.* **2016**, *688*, 840−848.

(21) Yang, J.-h.; Cheng, S.-h.; Wang, X.; Zhang, Z.; Liu, X.-r.; Tang, G.-h. Quantitative analysis of microstructure of carbon materials by HRTEM. *Trans. Nonferrous Met. Soc. China* **2006**, *16*, s796−s803.

(22) Zhang, J.; Hu, Y.; Jiang, X.; Chen, S.; Meng, S.; Fu, X. Design of a direct Z-scheme photocatalyst: Preparation and characterization of Bi_2O_3/g-C_3N_4 with high visible light activity. *J. Hazard. Mater.* **2014**, *280*, 713−722.

(23) Yao, B. D.; Chan, Y. F.; Zhang, X. Y.; Zhang, W. F.; Yang, Z. Y.; Wang, N. Formation mechanism of TiO_2 nanotubes. *Appl. Phys. Lett.* **2003**, *82*, 281−283.

https://doi.org/10.1021/acsomega.1c01068
ACS Omega 2021, 6, 12787−12793